ACS Infectious Diseases

pubs.acs.org/journal/aidcbc

Article

Structure-Guided Molecular Grafting of a Complex Broadly Neutralizing Viral Epitope

Goran Bajic, Max J. Maron, Timothy M. Caradonna, Ming Tian, Adam Mermelstein, Daniela Fera, Garnett Kelsoe, Masayuki Kuraoka, and Aaron G. Schmidt*

Cite This: https://dx.doi.org/10.1021/acsinfecdis.0c00008

Read Online

ACCESS | Metrics & More | Article Recommendations | Supporting Information

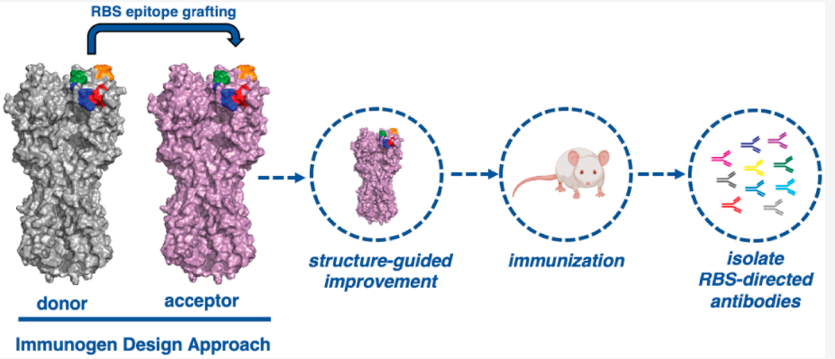

ABSTRACT: Antigenic variation and viral evolution have thwarted traditional influenza vaccination strategies. The broad protection afforded by a "universal" influenza vaccine may come from immunogens that elicit humoral immune responses targeting conserved epitopes on the viral hemagglutinin (HA), such as the receptor-binding site (RBS). Here, we engineered candidate immunogens that use noncirculating, avian influenza HAs as molecular scaffolds to present the broadly neutralizing RBS epitope from historical, circulating H1 influenzas. These "resurfaced" HAs (rsHAs) remove epitopes potentially targeted by strain-specific responses in immune-experienced individuals. Through structure-guided optimization, we improved two antigenically different scaffolds to bind a diverse panel of pan-H1 and H1/H3 cross-reactive bnAbs with high affinity. Subsequent serological and single germinal center B cell analyses from murine prime-boost immunizations show that the rsHAs are both immunogenic and can augment the quality of elicited RBS-directed antibodies. Our structure-guided, RBS grafting approach provides candidate immunogens for selectively presenting a conserved viral epitope.

KEYWORDS: *influenza hemagglutinin, immunogen design, protein engineering, broadly neutralizing antibodies*

Influenza evolves primarily at the human population level and within its animal reservoirs (swine and avian).[1] Influenza A viruses include 2 groups containing a total of 18 subtypes that are defined by genetic and serologic characteristics of the viral glycoproteins, hemagglutinin (HA) and neuraminidase (NA). Two influenza A subtypes, H1N1 and H3N2, and two influenza B lineages, Victoria and Yamagata, currently co-circulate in the human population.[1] Host humoral pressure, which predominantly targets the viral HA, selects for influenza mutations that render previous immune responses suboptimal. The humoral response then evolves, through immune memory and further B cell affinity maturation.[2−5] The net effect of this ongoing selection across the entire population exposed to the virus is a virus-immunity "arms race". The repeated exposure to influenza in the human population results in preexisting immunity which influences subsequent immune responses.[6−11] This immunological memory[12,13] presents a significant hurdle toward the development of a "universal" influenza vaccine. Strategies that both overcome the recall of refined, strain-specific responses and elicit broadly neutralizing antibodies (bnAbs) are necessary.

bnAbs against influenza HA target two relatively invariant epitopes, the receptor binding site (RBS) on the HA "head" and a surface along the HA "stem".[14] While stem-directed immunogens are in clinical development, efforts focusing on the RBS have lagged behind.[14] A significant challenge for RBS-directed immunogens is the presentation of the complex RBS structure that includes multiple segments, separated in linear sequence, but adjacent in conformational space.[15] While computational design of novel protein scaffolds has been

Received: January 8, 2020
Published: April 8, 2020

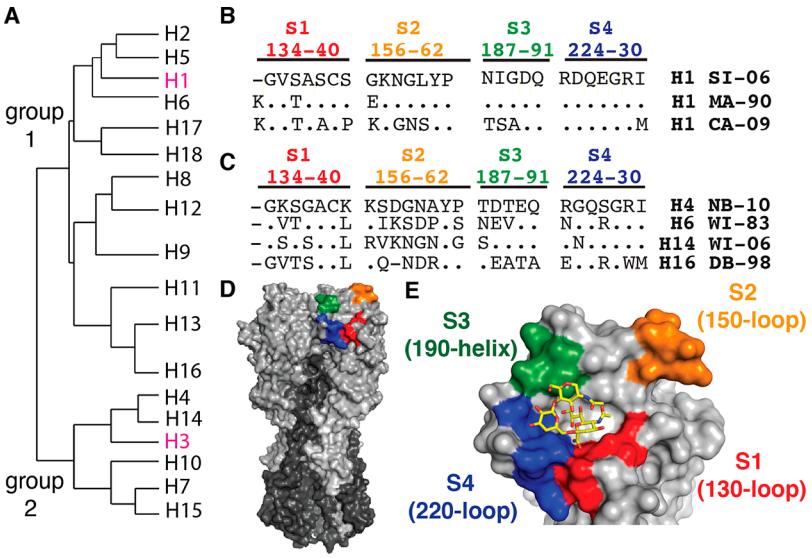

Figure 1. RBS grafts and sequence alignments. (A) Phylogeny of influenza subtypes. Group 1 and 2 influenzas are annotated. Highlighted in pink are the seasonal subtypes currently circulating in the human population. (B) Representative H1 antigenic clusters: H1 Massachusetts/1/1990 (MA-90), H1 Solomon Islands/03/2006 (SI-06), and H1 California/07/2009 (CA-09) are listed. Sequence alignment is in reference to SI-06, and conserved residues are marked as (.); segments defining the H1 RBS graft, S1−4, are colored. (C) Residues comprising S1−4 of the acceptor scaffolds (H3 numbering) from noncirculating influenzas H4 New Brunswick/00464/2010 (H4 NB-10), H6 Wisconsin/617/1983 (H6 WI-83), H14 Wisconsin/10OS3941/2006 (H14 WI-06), and H16 Delaware Bay/296/1998 (H16 DB-98). (D) Influenza HA trimer (PDB 5UGY) in surface representation. HA1 is in silver, HA2 is in dark gray, and S1−4 are colored. (E) LSTc (sialylneolacto-*N*-tetraose c, stick representation) modeled in complex with HA. S1−4 are colored, and HA is in silver.

Table 1. Affinity Measurements of rsHAs to a Panel of RBS-Directed Abs[a]

	CH67 V_H1−2	641 I-9 V_H4−59	H2526 V_H1−69	H2227 V_H4−4	K03.12 V_H1−2	C05 V_H3−23
H1 SI-06	0.57	0.67	0.56	0.39	0.83	1.1
H4 NB-10	>100	>100	>100	>100	>100	>100
H14 WI-10	>100	>100	>100	>100	>100	>100
rsH4NBv1	>100	>100	>100	>100	4.3	>100
rsH4NBv3	1.6	17.7	0.93	0.67	0.65	0.34
rsH14WIv1	9.5	>100	>100	>100	2.2	1.4
rsH14WIv2	0.31	2.7	0.20	1.0	1.1	0.065

[a] K_D's (in μM) were obtained by applying a 1:1 binding isotherm using vendor-supplied software with at least three independent concentrations. The V_H gene usages are listed for each antibody. K_D's beyond the limit of detection are reported as >100 μM. Values are for monomeric HA heads and Fabs.

done for HIV and RSV, the grafted epitopes were often less-complex (e.g., a single α helix).[16,17]

To overcome the significant hurdle of de novo protein design, we hypothesized that the RBS epitope from one HA subtype could be transplantable onto another antigenically distinct HA. We used noncirculating, avian influenza HAs as molecular scaffolds to present the RBS from circulating H1 influenzas. These resurfaced HA (rsHA) scaffolds present the H1 conserved RBS recognized by bnAbs and alter other epitopes targeted by strain-specific responses in immune-experienced individuals. The crystal structure of one scaffold in complex with a bnAb allowed for further structure-guided optimization of two antigenically distinct scaffolds to bind a diverse panel of pan-H1 and H1/H3 cross-reactive bnAbs. Immunization with a recombinant H1 HA followed by a single, heterologous boost with our rsHA immunogen showed comparable levels of RBS-directed antibody response to the H1 homologous prime-boost regimen. These data suggest that these rsHA immunogens, with further optimization of the vaccine regimen, may provide a pathway to a universal influenza vaccine, by exploiting the immunogenicity of the conserved RBS.

RESULTS

Grafting the H1 SI-06 RBS onto Acceptor HA Scaffolds. As a proof of principle, we chose the circulating H1 RBS epitope as the basis of a donor graft to scaffold onto HA subtypes not currently circulating in the human population (Figure 1a). H1 influenzas can be grouped into roughly three antigenic clusters with prototypical members represented by H1 Massachusetts/1/1990 (H1 MA-90), H1 Solomon Islands/03/06 (H1 SI-06), and H1 California/04/2009 (H1 CA-09) (Figures 1b and S1).[6] Importantly, bnAbs have been identified that can span these antigenic clusters (e.g., CH67,[18] 641 I-9,[19] Ab6649,[20] and 5J8[21]). We used the H1 SI-06 as the initial donor and defined four segments, S1−S4 (Figure 1b−e), comprising the RBS epitope for grafting (Figure 1b). These segments include 7 of the 13 critical residues that contact the receptor, sialic acid (Figure 1e); these 13 residues define the RBS "core" (Figure S1). Many of the remaining residues not included in the graft (e.g., Y95 and W153) are in the base of

https://dx.doi.org/10.1021/acsinfecdis.0c00008
ACS Infect. Dis. XXXX, XXX, XXX−XXX

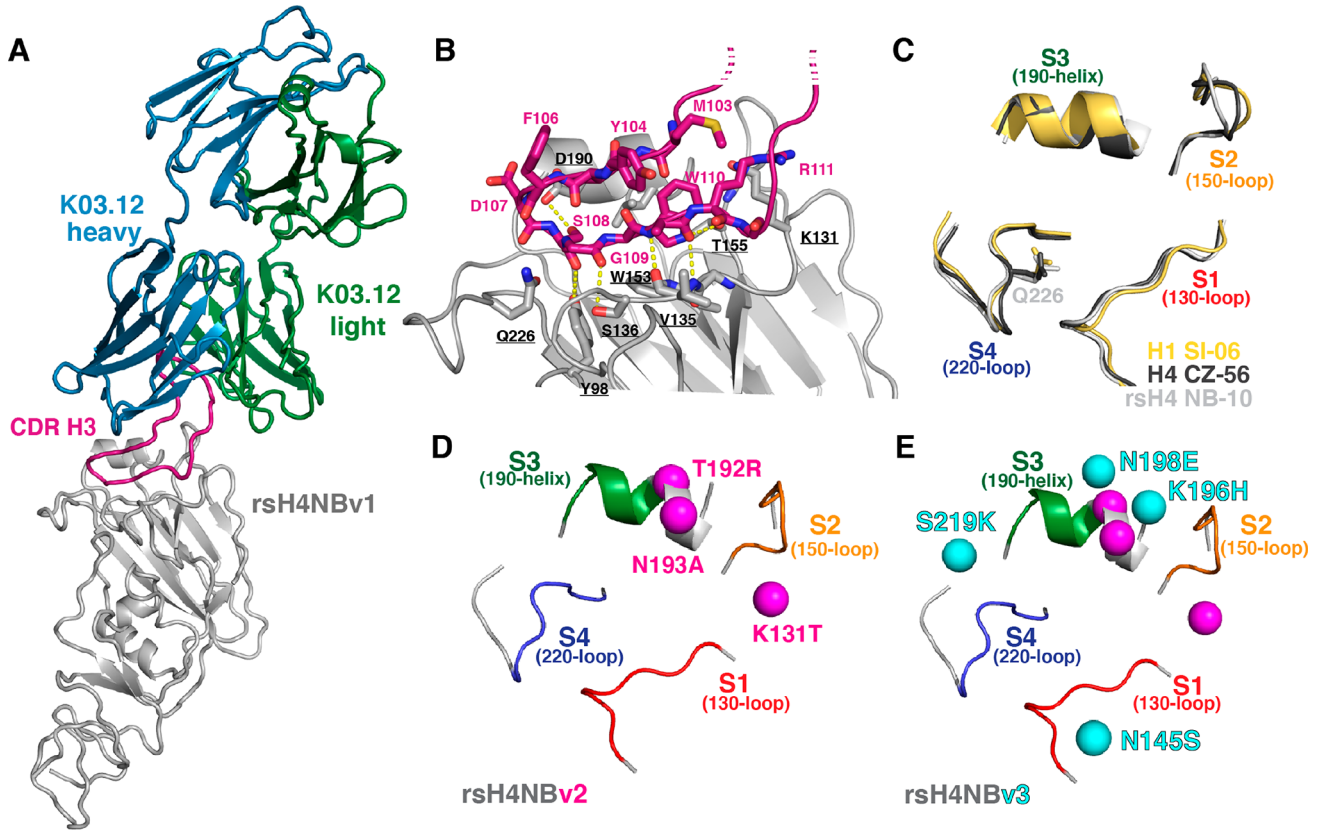

Figure 2. Structure of K03.12 in complex with rsH4NBv1 and scaffold improvement. (A) Antibody K03.12 Fab (heavy and light chains are colored blue and green, respectively) in complex with rsH4NBv1 HA1 "head" (silver). The CDR H3 (magenta) is marked. (B) Close-up of the antigen-binding site. The CDR H3 (magenta) is shown in sticks with key interacting HA residues (silver). Hydrogen bonds are denoted in yellow dashed-lines. (C) Comparison of the RBS of H1 SI-06, yellow (PDB 4YJZ); H4 A/duck/Czechoslovakia/1956 (H4 CZ-56), black (PDB 5XL3); and rsH4NBv1, silver. The segments of the grafts are labeled and colored. (D) rsH4NBv2 and (E) rsH4NBv3 with residues changed for each construct represented by a colored sphere. The original, unchanged segments from rsH4NBv1 are labeled and colored.

the RBS and they are nearly invariant across influenza subtypes. For the initial molecular scaffolds, we selected two noncirculating group 2 influenzas, H4N6 A/America black duck/New Brunswick/00464/2010 (H4 NB-10) and H14N6 A/mallard/Wisconsin/10OS3941/2010 (H14 WI-10). We selected them because they have little sequence similarity to circulating H1s (Figure S2). The acceptor HA S1−S4 boundaries were defined by aligning the H1 SI-06 sequence (Figure 1c). The rsHAs have the following nomenclature: "rsH4NBvX", the resurfaced (rs) HA scaffold subtype (H4), with an abbreviated strain name (NB) and different versions (vX). We could successfully overexpress the intergroup transfer of the H1 SI-06 RBS graft onto the H4 and H14 scaffolds, resulting in our first generation rsH4NBv1 and rsH14WIv1 scaffolds (Figure S3).

Binding Affinities of bnAbs to rsHAs. We determined the binding affinities of a panel of RBS-directed Fabs to these initial scaffolds by using biolayer interferometry (BLI). This panel included four pan-H1 (CH67, 641 I-9, H2526, and H2227) and two H1/H3 cross-reactive bnAbs (K03.12 and C05) that engage the RBS.[19,21−25] Each antibody has a footprint that overlaps with the RBS core but has different angles of approach and peripheral contacts (Figure S4). As seen in Table 1, neither scaffold bound all the RBS-directed Fabs. rsH4NBv1 bound only K03.12 with an equilibrium dissociation constant (K_D) ∼5.2× greater than that of wild-type H1 SI-06. rsH14WIv1 bound CH67, K03.12, and C05 with K_D's ∼17×, ∼2.7×, and ∼1.3× greater than that of wild-type H1 SI-06. None of the antibodies bound wild-type H4 NB-10 or H14 WI-10. These data suggest that there are peripheral residues in the first-generation scaffolds that impede bnAb binding and/or that the RBS graft is being presented in an altered conformation.

Structure of rsH4NBv1 in Complex with bnAb, K03.12. To identify further modifications on the first-generation scaffold that can be engineered to improve affinity to the bnAb panel, we determined the crystal structure of the rsH4NBv1 head in complex with the cross-reactive H1/H3 K03.12 antibody (Figure 2a, Table S1). Like the previously characterized C05 antibody, K03.12 engages the RBS with almost exclusively CDR H3-dependent contacts.[22] The antibody contacts 14 of the 26 residues in the S1−S4 RBS graft. Additional contacts are made with conserved residues critical for sialic acid interactions in the base of the RBS including Y95, W153, T155, and H183 (Figure 2b, H3 numbering). Comparison of the K03.12-rsH4NBv1 structure and the K03.12-H3 Texas/50/2012 complex shows a nearly identical approach with a slight twist and rocking of the V_H−V_L toward HA about the principal axis (Figure S5a, b).[23] The contacting residues within the antigen-combining sites between the two structures are nearly identical (Figure S5c, d). A comparison of the rsH4NBv1 HA to a wild-type H4 A/duck/Czechoslovakia/1956 (PDB 5XL3) and wild-type H1 SI-06 (PDB 5UGY) shows a displacement about S2 (150-loop)

https://dx.doi.org/10.1021/acsinfecdis.0c00008
ACS Infect. Dis. XXXX, XXX, XXX−XXX

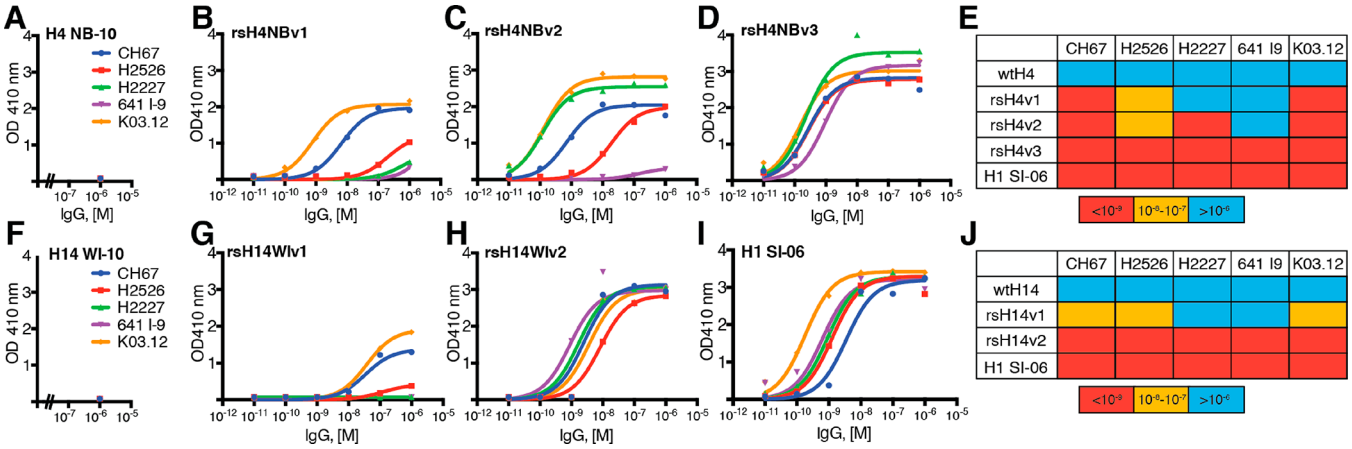

Figure 3. Reactivity of RBS-directed IgGs for rsHAs. CH67 (blue), H2526 (red), H2227 (green), 641 I-9 (violet), and K03.12 (orange) IgGs were titrated against (A) wild-type H4 NB-10, (B) rsH4NBv1, (D) rsH4NBv2, and (D) rsH4NBv3. (E) K_D's obtained from curves in (A)−(D) for H4 constructs displayed as a "heat map": warm colors are high affinity, and cool colors are low affinity. The legend is in M. IgG titrations for (F) wild-type H14 WI-10, (G) rsH14WIv1, (H) rsH14WIv2, and (I) control H1 SI-06 HA constructs. (J) K_D's obtained from curves in (F)−(I) for H14 constructs. ELISA measurements were done in duplicate over the concentration range except for (A) and (F), where only 1 μM final concentration of IgG was tested. The wild-type H1 SI-06 values in (E) and (J) are both derived from (I). Curve fitting was done with a nonlinear regression model, and K_D's were determined using GraphPad Prism version 8.0.

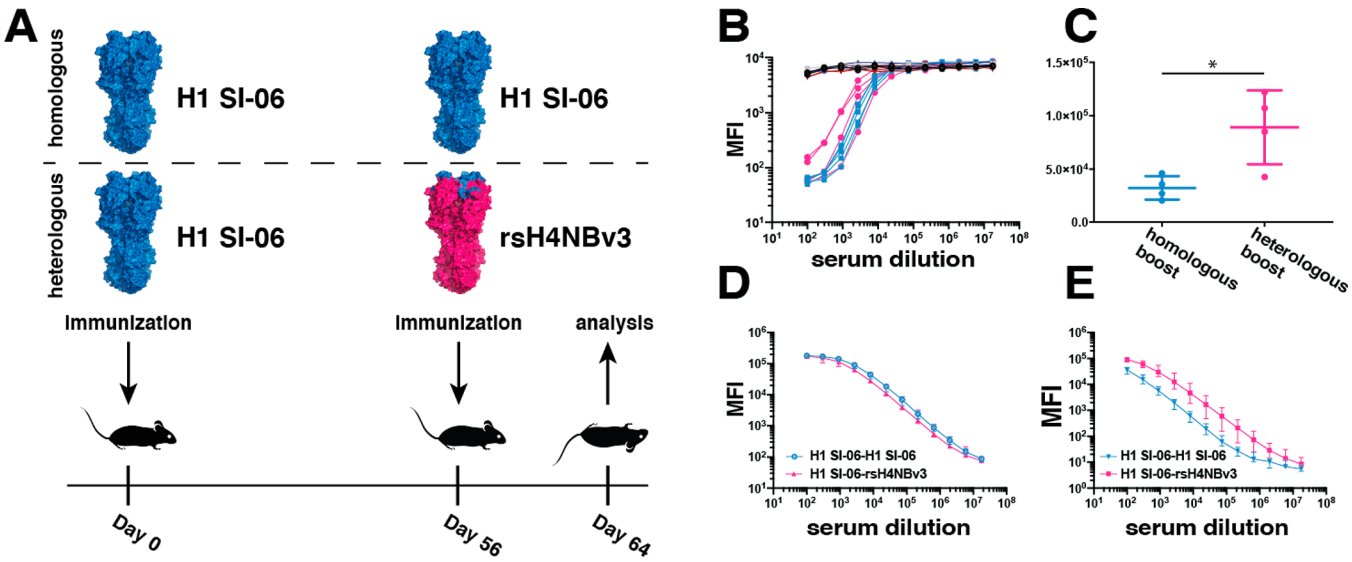

Figure 4. In vivo assessment of rsHA immunogenicity. (A) Schematic representation of the immunization strategy (B) CH67 competition to H1 SI-06 FLsE HA against the sera from wild-type nonimmunized B6 mice (black), J_H6 mice primed and boosted with H1 SI-06 (blue), and mice primed with H1 SI-06 and boosted with rsH4NBv3 (pink), (C) Total GC B cell counts in the animal cohorts. $n = 4$ mice for B6 and $n = 4$ mice for J_H6. *$p < 0.05$, Welch's t test. Error bars represent SD. (D) Serum reactivity against H1 SI-06. (E) Serum reactivity against rsH4NBv3. Mean values are plotted for (D) and (E) with error bars indicating SD.

with a shift of ∼3 Å; however, the overall conformation in the other grafted RBS segments is similar to that of the wild-type H1 SI-06 RBS (Figure 2c).

Structure-Guided Improvement of the rsHA Scaffolds. To improve scaffold binding to the RBS-directed bnAb panel, we docked the previously determined Fab structures onto the determined rsH4NBv1 structure to identify residues that may be modified to either alleviate steric clashes and/or reinforce interactions. We engineered two additional (scaffold) versions: (1) rsH4NBv2 had three mutations, K131T, T192R, and N193A (Figure 2d), and (2) rsH4NBv3 had four additional mutations, N145S, K196H, N198E, and S219 K (Figure 2e); no changes were made in the original grafted segments. We first assayed for scaffold improvement using an enzyme-linked immunosorbent assay (ELISA) (Figure 3). None of the antibodies bound to wild-type H4 NB-10 (Figure 3a) consistent with our BLI data using Fabs (Table 1). The second-generation scaffold increased affinity to four of the five Fabs (Figure 3b, c), while the third generation, rsH4NBv3, resulted in high-affinity binding to all five RBS-directed antibodies (Figure 3c). Based on this optimized rsH4NBv3 construct, we asked whether the same seven mutations could be made in context of the rsH14WIv1 scaffold to increase its affinity for the entire panel of RBS-directed antibodies. Indeed, when these mutations were engineered into rsH14WIv1, this optimized construct bound the entire panel of RBS-directed antibodies with high affinity (Figure 3g−i). For reference, H1

https://dx.doi.org/10.1021/acsinfecdis.0c00008
ACS Infect. Dis. XXXX, XXX, XXX−XXX

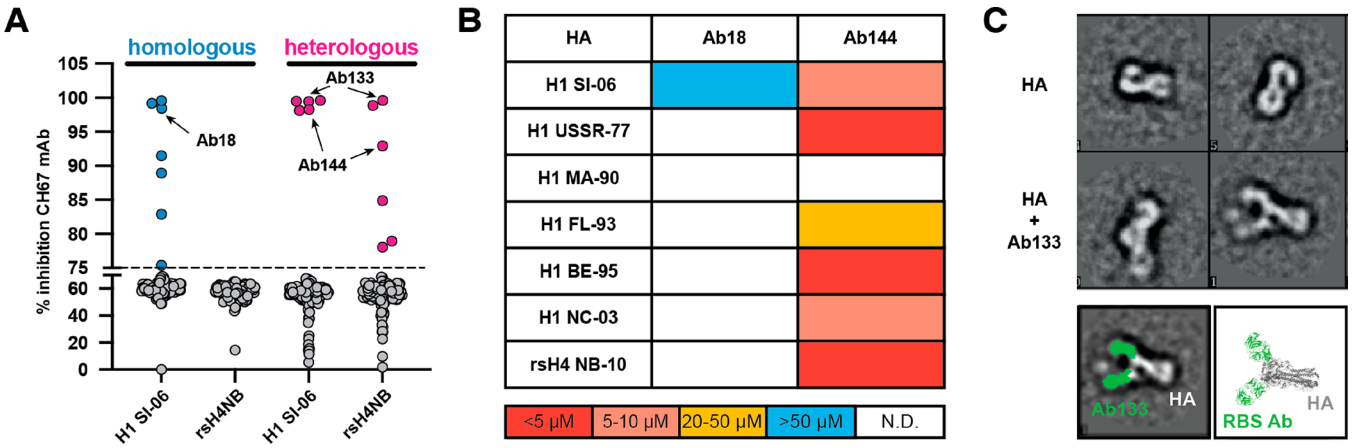

Figure 5. Identification and biochemical characterization of RBS-directed antibodies. (A) CH67 competition experiment against the single B cell culture supernatants from homologous (H1 SI-06; blue) and heterologous (H1 SI-06, rsH4NBv3; pink) immunizations. The competition was performed on Luminex beads coated with either H1 SI-06 or rsH4 NB-10, and antibody competition is expressed as percent of inhibition (*y*-axis); antibodies with >75% inhibition are colored. Representative monoclonal antibodies Ab18, Ab133, and Ab144 were selected for further characterization. (B) Binding to a panel of historical H1 HAs and the resurfaced rsH4 NB-10 was assayed with recombinant Fabs using biolayer interferometry. Affinity constants (K_D's, in μM) were obtained by applying a 1:1 binding isotherm using vendor-supplied software. The "heat map" color scheme is a visualization aid: warm colors are high affinity, and cool colors are low affinity. H1 SI-06, A/Solomon Islands/03/2006; H1 USSR-77, A/USSR/90/1977; H1MA-90, A/Massachusetts/1/1990; H1 FL-93, A/Florida/2/1993; H1 BE-95, A/Beijing/262/1995; H1 NC-03, A/North Carolina/3/2003; rsH4 NB-10, resurfaced duck/New Brunswick/00464/2010; N.D., nondetectable. (C) Visualization of the HA-Ab133 complex by negative stain electron microscopy. The top panels are of HA alone with and without cross-linking to Ab133 with glutaraldehyde. Ab133 is colored green in the bottom right panel and compared to a RBS antibody bound to HA (PDB ID: 5UG0). One copy of the RBS antibody is not shown for clarity.

SI-06 reactivity to the RBS-directed Ab panel is shown (Figure 3i). A summary of the K_D's is shown in Figure 3e, j.

Finally, we tested the optimized scaffolds in BLI to obtain more accurate K_D's, free of avidity effects present when using IgGs in ELISA. As seen in Table 1, both optimized scaffolds significantly increased affinities over their first-generation counterparts; rsHAs based on both optimized scaffolds bound all six bnAbs included in the panel. In particular, the rsH14WIv2 scaffold yielded affinities for CH67, H2526, and C05 even greater than those of wild-type H1 SI-06. In some cases (e.g., C05), the optimized resurfaced scaffold bound the Fab >10-fold more tightly than did wild-type H1 SI-06. In general, the rsH14WIv2 had affinities closest to that of the wild-type H1 SI-06. These data suggest a set of key residues, in addition to the initial RBS-donor grafts, that can be grafted onto other potential scaffolds to present an "optimized" epitope to bind (or elicit) a diverse set of RBS-directed bnAbs.

Serum and Germinal Center B Cell Responses to the rsHA Immunogen. To evaluate whether our rsHA immunogens can enrich for RBS-directed responses by allowing the expansion and differentiation of memory B cells, we first generated a knock-in (KI) mouse that has a human J_H6 and D2−2 segments (Figure S7 and Table S2). The human J_H6 and D2-2 segments were chosen to mimic two key features of observed human-RBS directed bnAbs that are absent in the wild-type C57BL/6 murine model: (1) a polytyrosine motif in the CDR H3 loop and (2) an overall CDR H3 length of 19−20 amino acids necessary for engaging the RBS.[19] We therefore immunized these generated mice (see Methods) with recombinant H1 SI-06 HA, to prime humoral immunity to a H1, and then boosted with our recombinant rsH4NBv3 (Figure 4a). We compared the resulting serum and germinal center (GC) responses originating from a homologous H1 SI-06/H1 SI-06 or a heterologous H1 SI-06/rsH4NBv3 prime/boost immunization. We found that, postboost, the serum IgG titers as well as the relative serum reactivity to the initial H1 SI-06 HA were comparable between the two cohorts (Figure S6a). To deconvolute the contribution of the H4 scaffold-dependent Abs, we performed a serum competition assay with H1 RBS-directed bnAb CH67 (Figure 4b) and found no demonstrable difference between the two cohorts. At the cellular level, we noted that the GC B cell frequencies were ∼3-fold higher in mice boosted with recombinant rsH4NBv3 (Figures 4c and S8). These data potentially point to disparities in immunogenicity between H1 SI-06 and rsH4NBv3 and highlight the apparent immunodominance of the H4 scaffold. To quantify the serum abundance of RBS-directed antibodies, we screened the sera from the two cohorts against H1 SI-06 and rsH4NBv3 HAs in a Luminex assay (Figure 4d, e). Sera from the heterologous immunization reacted more strongly with rsH4NBv3 (Figures 4e and S6b) and as strongly as those from the homologous one with H1 SI-06 (Figures 4d and S6c). These data highlight the immunogenicity of the resurfaced HA and its potential as a novel antigen.

Comparison of Single GC B Cell Responses to Wild-Type and Resurfaced HAs. To complement our serological study and to understand more fully HA RBS targeting, we assessed the reactivity of individual GC B cells isolated postimmunization using our single-cell Nojima culture system (Figure 5). We screened the culture supernatants from each immunization (homologous or heterologous) against both wild-type H1 SI-06 and rsH4 NB-10 in a competition assay with a known RBS-targeting mAb CH67 (Figure 5a). The competition was performed on Luminex beads, and the reduction in fluorescent signal, resulting from antibody competition, was expressed as percent of inhibition. We defined competitors as antibodies with 75% inhibition of CH67 mAb binding or greater. The data show that the homologous immunization (wild-type H1 SI-06 prime-boost) elicited 7 mAbs with such properties. Those mAbs competed

https://dx.doi.org/10.1021/acsinfecdis.0c00008
ACS Infect. Dis. XXXX, XXX, XXX−XXX

for CH67 binding only on wild-type H1 SI-06 and not on rsH4 NB-10 beads, suggesting that the footprint of these antibodies on HA extends beyond the minimal, conserved RBS present on both H1 SI-06 and rs H4 NB-10 making variable peripheral contacts. While the heterologous immunization elicited a comparable number of antibodies competing with CH67, five of six antibodies competed on both H1 SI-06 and rsH4 NB-10 beads, suggesting that these antibodies engage the minimal grafted RBS epitope, shared between the two HAs. These data point to qualitative differences between antibodies elicited by the two immunization regimens. To further characterize these potential differences, we asked whether there was a difference in breadth of binding to historical H1 HAs. We selected a representative antibody from each immunization group (Ab18, homologous; Ab144, heterologous immunization) to recombinantly express and to test for binding to an HA panel. Figure 5b shows binding data of this HA panel using Fabs and monomeric HA heads to avoid any avidity effects obtained from IgGs and trimeric HA FLsE. Ab18 bound only to the immunizing strain H1 SI-06 with modest affinity. However, Ab144 bound to H1 SI-06, rsH4 NB-10, as well as four additional historical H1 HAs with high affinity. Additionally, we obtained structural information on antibody Ab133 from the heterologous immunization that is clonally related to Ab144 (Figures 5A and S9C) by negative stain electron microscopy (EM). The EM 2D class averages show that the antibody binds to the RBS, in a similar way to other HA RBS antibodies[26] (Figures 5C and S9B); a stem-directed mAb FI6[27] is shown in Figure S9A for comparison. These data suggest that the heterologous immunization with our resurfaced immunogens offers an advantage over homologous immunization by eliciting antibodies with increased binding breadth; this is most likely a consequence of engaging only the conserved RBS epitope shared between the HAs and minimizing variable, peripheral contacts.

DISCUSSION

Current influenza research has focused on the development of a universal influenza vaccine. Such a vaccine should induce broad immunity (a) within seasonal, circulating H1 and H3 subtypes, (b) across subtypes (heterosubtypic), and (c) prepandemic (e.g., H5, H7). The pathway to achieving this broad protection will likely come from eliciting or boosting humoral responses to conserved sites on HA such as the RBS and "stem". Immunogen design strategies thus far have focused almost exclusively on targeting the conserved stem through either selectively displaying the HA2 stem[28−31] or using chimeric HAs that present circulating H1 or H3 stems with a heterologous HA1 "head."[14]

The data presented here show an alternative strategy for candidate immunogens to focus the immune response to the broadly neutralizing epitope of the RBS. Grafting of the H1 SI-06 RBS epitope onto two antigenically distinct HA scaffolds exploits the overall architecture of the HA protein circumventing the significant challenge in de novo protein scaffold design. Through structure-guided engineering, the optimized scaffolds bind a diverse panel of pan-H1 and H1/H3 cross-reactive RBS antibodies that represent the type of response one might wish to elicit by a universal influenza vaccine. Collectively, the bnAbs in the panel (Table 1) bind all H1 isolates both prepandemic (<2009) and postpandemic (>2009), as well as circulating H3N2 influenzas. Importantly, this collection of RBS-directed bnAbs tolerates the heterologous peripheries of the scaffolds surrounding the graft. These immunogens, therefore, would stimulate affinity maturation to refine humoral responses to the conserved, RBS core contacts shared between the scaffolds while adapting and accommodating antigenically distinct peripheries.

Our in vivo mouse immunization studies compared the resulting serum and GC responses from mice primed and boosted with either homologous or heterologous HA immunogens. Despite no discernible difference in a competition assay with bulk serum and a standard RBS-directed CH67 mAb, we noted that the heterologous immunization elicited more robust GC B cell responses, owing either to the influx of new, H4-specific clones and/or recall of the H1 RBS-specific memory B cells. Using single-cell isolation, we noted that, in the heterologous immunization regimen, very few B cells that were derived from secondary GCs reacted with the grafted RBS, consistent with a recent study on the frequency of memory B cell reentry to GCs.[32] We did, however, note that the antibodies elicited by the heterologous immunization bound to both the wild-type H1 SI-06 (from which the graft is derived) and the resurfaced HAs, indicating that they engage only the minimal, conserved RBS that minimize variable peripheral contacts. Consistent with this hypothesis, a representative antibody from the heterologous immunization had broader binding breadth to historical H1 HAs than did a representative antibody from the homologous control group. Although further studies involving fate labeling antigen-experienced cells and single-cell sequencing coupled with serum deconvolution will be necessary to better understand GC reentry and devise more optimal boosting strategies, our data highlight the benefit of boosting with the resurfaced HA to augment the quality of RBS-directed antibodies and mitigate strain-specific responses.

A significant hurdle for the development of a universal influenza vaccine is preexisting immunity present in the human population through either repeated seasonal vaccination or influenza infection. The HA scaffolds derive from avian influenzas that, to date, have not circulated in the human population and thus would likely avoid boosting strain-specific, memory recall responses in immune-experienced individuals. The strategy described here could be used to direct naïve immune responses to the conserved RBS through a prime-boost vaccine approach and/or could boost subdominant RBS-directed bnAbs already present in immune-experienced individuals.[11,19] More generally, the immunogen design approach of epitope grafting could be used for other rapidly evolving pathogens for which preexisting immunity is present (e.g., RSV and dengue).

METHODS

Expression and Purification of HA. rHA1 "head" and rHA full length soluble ectodomains (FLsE) constructs were cloned into the pFastBac vector for insect cell expression (Hi5 cells) or pVRC vector for mammalian expression (HEK293F cells). HAs were derived from the following templates: A/America black duck/New Brunswick/00464/2010 (H4N6) (GenBank: AGG81749.1) and A/mallard/Wisconsin/10OS3941/2010 (H14N6) (GenBank: AGE03043) (Table S3). All constructs were confirmed by DNA sequencing at the DNA Sequencing Core Facility at Dana Farber Cancer Institute. For biolayer interferometry (BLI) and crystallography, the HA1 head constructs contained a HRV 3C-cleavable C-terminal His_{6X} tag or SBP-His_{8X} tag. The HA FLsE

https://dx.doi.org/10.1021/acsinfecdis.0c00008
ACS Infect. Dis. XXXX, XXX, XXX−XXX

constructs used in ELISA assays contained a thrombin or HRV 3C-cleavable C-terminal foldon tag with either a His_{6X} or SBP-His_{8X} tag. All constructs were purified from supernatants by passage over Cobalt-TALON resin (Takara) followed by gel filtration chromatography on Superdex 200 Increase columns (GE Healthcare) in 10 mM Tris-HCl, 150 mM NaCl at pH 7.5. For BLI and crystallography, the tags were removed using HRV 3C protease (ThermoScientific) and the protein was repurified using Cobalt-TALON resin to remove the protease, tag, and noncleaved protein.

Fab and IgG Expression and Purification. For Fab and IgG production, the genes for the heavy- and light-chain variable domains were synthesized and codon optimized by Integrated DNA Technologies and subcloned into pVRC protein expression vectors containing human heavy- and light-chain constant domains, as previously described.[11,19] Heavy-chain constructs for Fab production contained a noncleavable His_{6X} tag; for IgG heavy constructs, there was no cleavable purification tag. Constructs were confirmed by sequencing at the DNA Sequencing Core Facility at Dana Farber Cancer Institute. Fabs and IgGs were produced by transient transfection in suspension 293F or adherent HEK 293T cells using Lipofectamine 2000 (Invitrogen) or polyethylenimine (PEI). Supernatants were harvested 4−5 days later and clarified by centrifugation. Fabs were purified using Cobalt-TALON resin (Takara) followed by gel filtration chromatography on Superdex 200 Increase columns (GE Healthcare) in 10 mM Tris-HCl, 150 mM NaCl at pH 7.5. IgGs were purified using Protein G Plus agarose (ThermoFisher Scientific). Briefly, IgG supernatants were incubated overnight with agarose slurry, eluted with 0.1 M glycine, pH 2.5, normalized with 1 M Tris-HCl, pH 8.0, and dialyzed against PBS buffer overnight.

Crystallization and Data Collection. rsH4NBv1 HA1 head domain and K03.12 Fab (both expressed in HEK293F cells) were incubated at 1:1.5 molar ratio, respectively. The complex was isolated by size exclusion chromatography using a 24 mL Superdex Increase column equilibrated in 10 mM Tris-HCl, 150 mM NaCl. Crystallization was achieved by hanging drop vapor diffusion at 18 °C. Crystals were grown in 100 mM sodium citrate (pH 4.5), 20% (wt/vol) PEG 4000. Crystals were cryoprotected in mother liquor supplemented with 25% (v/v) glycerol and flash-frozen in liquid nitrogen. Data were collected at 0.999 Å with a rotation of 1° per image on the 8.2.2 beamline, Advanced Light Source, at Berkeley National Laboratory.

Structure Determination and Analysis. X-ray diffraction data were processed with XDS.[33] The structure was determined by molecular replacement using PHASER[34,35] with the K03.12-A/Texas/50/2012 (H3N2)-head complex (PDB ID 5W08) as a search model.[23] Density-modified, NCS-averaged electron density maps were generated with DM (CCP4) and were used as a guide for model building. Individual coordinate and group B factor refinement was performed using PHENIX.[36] Model building was done in COOT[37] and assessed with MolProbity.[38] N-Linked glycan stereochemistry was validated with Privateer.[39] Figures were generated using PyMOL Molecular Graphics System (v1.8.0.0; Schrödinger LLC).

Negative Stain EM. Purified SI-06 FLsE trimer was incubated with a 6-fold molar excess of FI6 Fab at 4 °C for 1 h and run over a Superpose 6 Increase column (GE Healthcare) in a buffer of 5 mM HEPES, pH 7.5, 150 mM NaCl. Size exclusion chromatography was not run with Ab133 for initial imaging to prevent Ab133 from dissociating. To keep Ab133 bound, we cross-linked by addition of 0.5% glutaraldehyde (GLA; Electron Microscopy Sciences) at 4 °C for 1 h, after which the reaction was stopped by addition of 75 mM Tris buffer (pH 7.4) and then run over the Superpose 6 Increase column (GE Healthcare). Fractions containing complex were concentrated to 0.01 mg/mL. A 2.5 μL aliquot of the complex was applied for 30 s onto a carbon-coated 400 Cu mesh grid that had been glow discharged at 5 mA for 2 min, followed by negative staining with 0.7% uranyl formate for 20 s. Samples were imaged using a FEI Tecnai T12 microscope operated at 100 kV and a magnification of ∼52 000×, yielding a pixel size of 1.66 Å at the specimen plane. Images were acquired with a Gatan 4k × 4k OneView camera using a nominal defocus of 1500 nm at 0°. Particles were picked with EMAN2 and put into a particle stack.

Interferometry Binding Experiments. Interferometry experiments were performed using a BLItz instrument (fortéBIO, Pall Corporation). Fabs were immobilized on a Ni-NTA biosensor and cleaved rHA heads (made in insect Hi5 cells) were titrated to obtain binding affinities. Initial, single-hit concentrations were tested at 35 μM for binding and then subsequent titrations for at least three different concentrations (chosen depending on the apparent K_D from the high concentration); the refined K_D was obtained through global fit of the titration curves by applying a 1:1 binding isotherm using vendor-supplied software. All experiments were performed in 10 mM Tris-HCl, 150 mM NaCl at pH 7.5 and at room temperature.

ELISA. Amounts of 5−10 ng of rHA FLsE expressed in insect Hi5 cells were adhered to high-capacity binding, 96-well plates (Corning) overnight in PBS. Plates were blocked with nonfat dried milk in PBS containing Tween-20 (PBS-T) for 1 h at room temperature (RT). Blocking solution was discarded and 10-fold dilutions of RBS-directed IgGs in PBS were added to wells and incubated for 1 h at RT. Plates were then washed three times with PBS-T. Secondary anti-human IgG-HRP (Abcam), in PBS-T, was added to each plate and incubated for 1 h at RT. Plates were then washed three times with PBS-T. Plates were developed using 1-Step ABTS substrate (ThermoFisher) and immediately read using a plate reader at 410 nm. Data were plotted using Prism 8 (GraphPad Software) and affinities determined by applying a nonlinear regression model.

Mice. C57BL/6 mice were obtained from the Jackson Laboratory. J_H6 mice were generated as described below. Mice were bred and maintained under specific pathogen-free conditions at the Duke University Animal Care Facility. Mouse immunization experiments were conducted per the approved protocol by the Duke University Institutional Animal Care and Use Committee.

Generation of Human J_H6 Murine Model. In the human J_H6 mouse model, human J_H6 replaces mouse J_H1−J_H4 and human D2-2 replaces the mouse DQ52 segment. The choice of human J_H6 and D2-2 was based on the observation that a substantial fraction of human anti-RBS antibodies utilize these gene segments in CDR H3. To generate the hJ_H6 mouse line, a targeting construct containing the hD2-2 and hJ_H6 cassette was transfected into a F1 ES cell line that was derived from a cross between the 129/Sv strain and the C57BL/6 strain mice. The cassette was integrated into the mouse DQ52-J_H6 locus via homologous integration. The homology arm was derived from genomic DNA from the C57BL/6 mouse strain. Due to sequence polymorphisms between the 129/Sv mouse strain

https://dx.doi.org/10.1021/acsinfecdis.0c00008
ACS Infect. Dis. XXXX, XXX, XXX−XXX

and C57BL/6 strain, homologous recombination preferentially integrated the hD2-2 and hJ_H6 cassette into the IgH^b allele in the ES cell. The ES clone was injected into mouse Rag2 deficient blastocysts to generate chimeric mice. Because Rag2 is essential to V(D)J recombination, all the B and T cells were derived from the injected ES cells, and the chimeric mice can be used directly for analysis. The method is referred to as Rag2 deficient blastocyst complementation.[40] Figure S7 shows analysis of the B cells in this type of chimeric mice, as compared with a WT control mouse of mixed 129/Sv and C57BL/6 genetic background. For this analysis, splenic B cells were stained with fluorophore conjugated antibodies, as indicated next to the FACS plots. To analyze the V_H, D, and J_H usage in the Ig heavy chains from IgM^b B cells (Table S2), IgM^b B cells were sorted by FACS,and 5′RACE was performed to generate a library of μ heavy chains expressed by the sorted B cells. The PCR products were cloned into pGEXT-easy vector, and some of the cloned PCR products were sequenced. The identities of the V_H, D, and J_H segments were determined by Ig Blast.

Immunizations. J_H6 mice (female, 8−12 weeks old) were immunized with 20 μg of H1 SI-06 HAs, expressed in insect Hi5 cells, in Alhydrogel via footpad. Eight weeks later, cohorts of mice were boosted with 20 μg of either H1 SI-06 HAs or rsH4NBv3 HAs in Alhydrogel via hock. Mice were sacrificed 8 days after prime or boost immunizations, respectively, and the draining, popliteal lymph nodes, and sera were collected to measure GC and antibody responses, respectively.

Flow Cytometry. GC B cells ($GL\text{-}7^+B220^{hi}CD38^{lo}\text{-}IgD^-CD93^-CD138^-$) and plasmablasts/-cytes ($B220^{lo}CD138^{hi}$) cells in popliteal LNs were determined as described.[41,42] Labeled cells were analyzed/sorted in a FACS Canto (BD Bioscience) or a FACS Vantage with DIVA option (BD Bioscience). Flow cytometric data were analyzed with FlowJo software (Treestar Inc.). Doublets were excluded by FSC-A/FSC-H gating strategy. Cells that take up propidium iodide were excluded from our analyses.

Nojima Culture. Single B cell cultures were performed as described.[42] Briefly, single GC B cells were sorted for their phenotype and cultured for 10 days in the presence of NB-21.2D9 feeder cells. After culture, the supernatants were harvested for Luminex assays and culture plates were stored at −80 °C for V(D)J amplifications.

BCR Sequencing. V(D)J rearrangements of cultured B cells were amplified by a nested PCR, cloned, and sequenced as previously described.[42] The rearranged V, D, and J gene segments were identified using IMGT/V-QUEST (http://www.imgt.org/).

Luminex Multiplex Assay. Reactivity of clonal IgGs in culture supernatants and of mouse sera was determined by Luminex multiplex assay with modifications.[41] Briefly, mixtures of antigen-conjugated (H1 SI-06 or rsH4NBv3 HAs, both FLsE, made in insect Hi5 cells) microspheres were incubated with serially diluted serum samples for 2 h at room temperature or overnight at 4 °C (for competition assay) with mild agitation. Samples were diluted in PBS containing 1% cow milk, 1% BSA, 0.05% Tween 20, and 0.05% NaN_3. For competition, human monoclonal IgG1 CH67 (2 ng/mL) was added to the plates without washing and plates were incubated for 2 h at room temperature with mild agitation. After washing, PE goat anti-mouse IgG or PE mouse anti-human IgG (both from Southern Biotech, the latter for competition assay) was added to the plates and incubated for 1 h at room temperature with mild agitation. After washing, microspheres were resuspended in PBS containing 1% BSA, 0.05% Tween 20, and 0.05% NaN_3 and fluorescent signals from each microsphere were measured in a Bio-Plex 3D machine (Bio-Rad).

■ ASSOCIATED CONTENT

Supporting Information

The Supporting Information is available free of charge at https://pubs.acs.org/doi/10.1021/acsinfecdis.0c00008.

Sequence alignment of historical H1 RBS and critical residues comprising sialic acid contacts; conservation mapping onto HA structure; biochemical characterization of the optimized rsHA; intermolecular contacts (footprints) of RBS-directed antibodies; structural comparison of mAb K03.12 bound with rsH4NBv1 and H3 TX-12; total IgG titer measurements; illustration showing the integration of human D2-2*01 (hD2-2*01) and human J_H6*03 (hJ_H6*03) segments into the mouse IgH locus; flow cytometry gating; 2D class averages from negative stain EM for HA in complex with the stem antibody, FI6, as well as a portion of a raw negative stain EM micrograph; crystallographic data collection and model refinement statistics; VH, D, and JH usage of IgMb B cells; protein sequences of the different HA constructs (PDF)

■ AUTHOR INFORMATION

Corresponding Author

Aaron G. Schmidt − *Ragon Institute of MGH, MIT and Harvard, Cambridge, Massachusetts 02139, United States; Department of Microbiology, Harvard Medical School, Boston, Massachusetts 02115, United States*; Phone: 857-268-7118; Email: aschmidt@crystal.harvard.edu

Authors

Goran Bajic − *Laboratory of Molecular Medicine, Boston Children's Hospital and Department of Pediatrics, Harvard Medical School, Boston, Massachusetts 02115, United States;* orcid.org/0000-0003-0480-4324

Max J. Maron − *Ragon Institute of MGH, MIT and Harvard, Cambridge, Massachusetts 02139, United States*

Timothy M. Caradonna − *Laboratory of Molecular Medicine, Boston Children's Hospital, Harvard Medical School, Boston, Massachusetts 02115, United States; Ragon Institute of MGH, MIT and Harvard, Cambridge, Massachusetts 02139, United States*

Ming Tian − *Program in Cellular and Molecular Medicine, Boston Children's Hospital, Harvard Medical School, Boston, Massachusetts 02115, United States*

Adam Mermelstein − *Department of Chemistry and Biochemistry, Swarthmore College, Swarthmore, Pennsylvania 19081, United States*

Daniela Fera − *Department of Chemistry and Biochemistry, Swarthmore College, Swarthmore, Pennsylvania 19081, United States*

Garnett Kelsoe − *Duke Human Vaccine Institute and Department of Immunology, Duke University, Durham, North Carolina 27710, United States*

Masayuki Kuraoka − *Department of Immunology, Duke University, Durham, North Carolina 27710, United States*

Complete contact information is available at: https://pubs.acs.org/10.1021/acsinfecdis.0c00008

https://dx.doi.org/10.1021/acsinfecdis.0c00008
ACS Infect. Dis. XXXX, XXX, XXX−XXX

Author Contributions

A.G.S. designed research; G.B., M.J.M., T.M.C., M,T., M.K., A.M., D.F., and A.G.S. performed research; G.B., G.K., M.K., and A.G.S. analyzed data; G.B. and A.G.S. wrote the paper. G.B., M.J.M., T.M.C., M.T., D.F., G.K., and M.K. edited and commented on the paper.

Notes

The authors declare the following competing financial interest(s): A.G.S., G.B., and M.J.M. have filed a patent application regarding the work published in this paper.

Coordinates and structure factors have been deposited in the Protein Data Bank under accession code PDB 6UR5 for the rsH4NBv1-K03.12 complex.

■ ACKNOWLEDGMENTS

D. Fera was supported by Swarthmore College Startup and Faculty funds. We thank the Electron Microscopy Resource Lab (EMRL) at the Perelman School of Medicine, University of Pennsylvania, for access to instrumentation and its staff for assistance and training. We thank Stephen Harrison and members of his laboratory at Harvard Medical School for helpful discussions, in particular Kevin McCarthy. We thank Wenli Zhang, Dongmei Liao, and Xiaoe Liang at Duke University for technical assistance and mouse colony maintenance. BLI affinity measurements were carried out in the Center for Macromolecular Interactions at Harvard Medical School, directed by Kelly Arnett. We thank the beamline staff at the Advanced Light Source (Lawrence Berkeley Laboratory), beamline 8.2.2, for assistance with the recording of X-ray diffraction data. We thank Yoana Dimitrova for help with X-ray data processing. Sequencing reactions were carried out with an ABI3730xl DNA analyzer at the DNA Resource Core of Dana-Farber/Harvard Cancer Center (funded in part by NCI Cancer Center support Grant 2P30CA006516-48). This research was supported by NIH Grants P01 AI089618 (to S. C. Harrison), U19 AI117892 (to G. Kelsoe), and R01 AI146779 (to A.G. Schmidt). The project described was supported by Award Number T32GM007753 from the National Institute of General Medical Sciences. The content is solely the responsibility of the authors and does not necessarily represent the official views of the National Institute of General Medical Sciences or the National Institutes of Health.

■ REFERENCES

(1) Taubenberger, J. K., and Morens, D. M. (2010) Influenza: the once and future pandemic. *Public Health Rep. 125* (Suppl 3), 15−26.

(2) Dal Porto, J. M., Haberman, A. M., Shlomchik, M. J., and Kelsoe, G. (1998) Antigen drives very low affinity B cells to become plasmacytes and enter germinal centers. *J. Immunol 161* (10), 5373−81.

(3) De Silva, N. S., and Klein, U. (2015) Dynamics of B cells in germinal centres. *Nat. Rev. Immunol. 15* (3), 137−48.

(4) Foote, J., and Milstein, C. (1991) Kinetic maturation of an immune response. *Nature 352* (6335), 530−2.

(5) Victora, G. D., and Nussenzweig, M. C. (2012) Germinal centers. *Annu. Rev. Immunol. 30*, 429−57.

(6) Bedford, T., Suchard, M. A., Lemey, P., Dudas, G., Gregory, V., Hay, A. J., McCauley, J. W., Russell, C. A., Smith, D. J., and Rambaut, A. (2014) Integrating influenza antigenic dynamics with molecular evolution. *eLife 3*, No. e01914.

(7) Fonville, J. M., Wilks, S. H., James, S. L., Fox, A., Ventresca, M., Aban, M., Xue, L., Jones, T. C., Le, N. M., Pham, Q. T., Tran, N. D., Wong, Y., Mosterin, A., Katzelnick, L. C., Labonte, D., Le, T. T., van der Net, G., Skepner, E., Russell, C. A., Kaplan, T. D., Rimmelzwaan, G. F., Masurel, N., de Jong, J. C., Palache, A., Beyer, W. E., Le, Q. M., Nguyen, T. H., Wertheim, H. F., Hurt, A. C., Osterhaus, A. D., Barr, I. G., Fouchier, R. A., Horby, P. W., and Smith, D. J. (2014) Antibody landscapes after influenza virus infection or vaccination. *Science 346* (6212), 996−1000.

(8) Hensley, S. E. (2014) Challenges of selecting seasonal influenza vaccine strains for humans with diverse pre-exposure histories. *Curr. Opin. Virol. 8*, 85−9.

(9) Li, Y., Myers, J. L., Bostick, D. L., Sullivan, C. B., Madara, J., Linderman, S. L., Liu, Q., Carter, D. M., Wrammert, J., Esposito, S., Principi, N., Plotkin, J. B., Ross, T. M., Ahmed, R., Wilson, P. C., and Hensley, S. E. (2013) Immune history shapes specificity of pandemic H1N1 influenza antibody responses. *J. Exp. Med. 210* (8), 1493−500.

(10) Moody, M. A., Zhang, R., Walter, E. B., Woods, C. W., Ginsburg, G. S., McClain, M. T., Denny, T. N., Chen, X., Munshaw, S., Marshall, D. J., Whitesides, J. F., Drinker, M. S., Amos, J. D., Gurley, T. C., Eudailey, J. A., Foulger, A., DeRosa, K. R., Parks, R., Meyerhoff, R. R., Yu, J. S., Kozink, D. M., Barefoot, B. E., Ramsburg, E. A., Khurana, S., Golding, H., Vandergrift, N. A., Alam, S. M., Tomaras, G. D., Kepler, T. B., Kelsoe, G., Liao, H. X., and Haynes, B. F. (2011) H3N2 influenza infection elicits more cross-reactive and less clonally expanded anti-hemagglutinin antibodies than influenza vaccination. *PLoS One 6* (10), No. e25797.

(11) Schmidt, A. G., Do, K. T., McCarthy, K. R., Kepler, T. B., Liao, H. X., Moody, M. A., Haynes, B. F., and Harrison, S. C. (2015) Immunogenic Stimulus for Germline Precursors of Antibodies that Engage the Influenza Hemagglutinin Receptor-Binding Site. *Cell Rep. 13* (12), 2842−50.

(12) Davenport, F. M., Hennessy, A. V., and Francis, T., Jr. (1953) Epidemiologic and immunologic significance of age distribution of antibody to antigenic variants of influenza virus. *J. Exp. Med. 98* (6), 641−56.

(13) Jensen, K. E., Davenport, F. M., Hennessy, A. V., and Francis, T., Jr. (1956) Characterization of influenza antibodies by serum absorption. *J. Exp. Med. 104* (2), 199−209.

(14) Krammer, F., and Palese, P. (2015) Advances in the development of influenza virus vaccines. *Nat. Rev. Drug Discovery 14* (3), 167−82.

(15) Skehel, J. J., and Wiley, D. C. (2000) Receptor binding and membrane fusion in virus entry: the influenza hemagglutinin. *Annu. Rev. Biochem. 69*, 531−69.

(16) Ofek, G., Guenaga, F. J., Schief, W. R., Skinner, J., Baker, D., Wyatt, R., and Kwong, P. D. (2010) Elicitation of structure-specific antibodies by epitope scaffolds. *Proc. Natl. Acad. Sci. U. S. A. 107* (42), 17880−7.

(17) Correia, B. E., Bates, J. T., Loomis, R. J., Baneyx, G., Carrico, C., Jardine, J. G., Rupert, P., Correnti, C., Kalyuzhniy, O., Vittal, V., Connell, M. J., Stevens, E., Schroeter, A., Chen, M., Macpherson, S., Serra, A. M., Adachi, Y., Holmes, M. A., Li, Y., Klevit, R. E., Graham, B. S., Wyatt, R. T., Baker, D., Strong, R. K., Crowe, J. E., Jr., Johnson, P. R., and Schief, W. R. (2014) Proof of principle for epitope-focused vaccine design. *Nature 507* (7491), 201−6.

(18) Schmidt, A. G., Xu, H., Khan, A. R., O'Donnell, T., Khurana, S., King, L. R., Manischewitz, J., Golding, H., Suphaphiphat, P., Carfi, A., Settembre, E. C., Dormitzer, P. R., Kepler, T. B., Zhang, R., Moody, M. A., Haynes, B. F., Liao, H. X., Shaw, D. E., and Harrison, S. C. (2013) Preconfiguration of the antigen-binding site during affinity maturation of a broadly neutralizing influenza virus antibody. *Proc. Natl. Acad. Sci. U. S. A. 110* (1), 264−9.

(19) Schmidt, A. G., Therkelsen, M. D., Stewart, S., Kepler, T. B., Liao, H. X., Moody, M. A., Haynes, B. F., and Harrison, S. C. (2015) Viral receptor-binding site antibodies with diverse germline origins. *Cell 161* (5), 1026−34.

(20) Raymond, D. D., Bajic, G., Ferdman, J., Suphaphiphat, P., Settembre, E. C., Moody, M. A., Schmidt, A. G., and Harrison, S. C. (2018) Conserved epitope on influenza-virus hemagglutinin head defined by a vaccine-induced antibody. *Proc. Natl. Acad. Sci. U. S. A. 115* (1), 168−173.

https://dx.doi.org/10.1021/acsinfecdis.0c00008
ACS Infect. Dis. XXXX, XXX, XXX−XXX

(21) Hong, M., Lee, P. S., Hoffman, R. M., Zhu, X., Krause, J. C., Laursen, N. S., Yoon, S. I., Song, L., Tussey, L., Crowe, J. E., Jr., Ward, A. B., and Wilson, I. A. (2013) Antibody recognition of the pandemic H1N1 Influenza virus hemagglutinin receptor binding site. *Journal of virology 87* (22), 12471−80.
(22) Ekiert, D. C., Kashyap, A. K., Steel, J., Rubrum, A., Bhabha, G., Khayat, R., Lee, J. H., Dillon, M. A., O'Neil, R. E., Faynboym, A. M., Horowitz, M., Horowitz, L., Ward, A. B., Palese, P., Webby, R., Lerner, R. A., Bhatt, R. R., and Wilson, I. A. (2012) Cross-neutralization of influenza A viruses mediated by a single antibody loop. *Nature 489* (7417), 526−32.
(23) McCarthy, K. R., Watanabe, A., Kuraoka, M., Do, K. T., McGee, C. E., Sempowski, G. D., Kepler, T. B., Schmidt, A. G., Kelsoe, G., and Harrison, S. C. (2018) Memory B Cells that Cross-React with Group 1 and Group 2 Influenza A Viruses Are Abundant in Adult Human Repertoires. *Immunity 48* (1), 174−184.
(24) Whittle, J. R., Zhang, R., Khurana, S., King, L. R., Manischewitz, J., Golding, H., Dormitzer, P. R., Haynes, B. F., Walter, E. B., Moody, M. A., Kepler, T. B., Liao, H. X., and Harrison, S. C. (2011) Broadly neutralizing human antibody that recognizes the receptor-binding pocket of influenza virus hemagglutinin. *Proc. Natl. Acad. Sci. U. S. A. 108* (34), 14216−21.
(25) McCarthy, K. R., Raymond, D. D., Do, K. T., Schmidt, A. G., and Harrison, S. C. (2019) Affinity maturation in a human humoral response to influenza hemagglutinin. *Proc. Natl. Acad. Sci. U. S. A. 116* (52), 26745−26751.
(26) Liu, Y., Pan, J., Jenni, S., Raymond, D. D., Caradonna, T., Do, K. T., Schmidt, A. G., Harrison, S. C., and Grigorieff, N. (2017) CryoEM Structure of an Influenza Virus Receptor-Binding Site Antibody-Antigen Interface. *J. Mol. Biol. 429* (12), 1829−1839.
(27) Corti, D., Voss, J., Gamblin, S. J., Codoni, G., Macagno, A., Jarrossay, D., Vachieri, S. G., Pinna, D., Minola, A., Vanzetta, F., Silacci, C., Fernandez-Rodriguez, B. M., Agatic, G., Bianchi, S., Giacchetto-Sasselli, I., Calder, L., Sallusto, F., Collins, P., Haire, L. F., Temperton, N., Langedijk, J. P., Skehel, J. J., and Lanzavecchia, A. (2011) A neutralizing antibody selected from plasma cells that binds to group 1 and group 2 influenza A hemagglutinins. *Science 333* (6044), 850−6.
(28) Yassine, H. M., Boyington, J. C., McTamney, P. M., Wei, C. J., Kanekiyo, M., Kong, W. P., Gallagher, J. R., Wang, L., Zhang, Y., Joyce, M. G., Lingwood, D., Moin, S. M., Andersen, H., Okuno, Y., Rao, S. S., Harris, A. K., Kwong, P. D., Mascola, J. R., Nabel, G. J., and Graham, B. S. (2015) Hemagglutinin-stem nanoparticles generate heterosubtypic influenza protection. *Nat. Med. 21* (9), 1065−70.
(29) Sagawa, H., Ohshima, A., Kato, I., Okuno, Y., and Isegawa, Y. (1996) The immunological activity of a deletion mutant of influenza virus haemagglutinin lacking the globular region. *J. Gen. Virol. 77* (Pt 7), 1483−7.
(30) Steel, J., Lowen, A. C., Wang, T. T., Yondola, M., Gao, Q., Haye, K., Garcia-Sastre, A., and Palese, P. (2010) Influenza virus vaccine based on the conserved hemagglutinin stalk domain. *mBio 1* (1), e00018-10.
(31) Boyoglu-Barnum, S., Hutchinson, G. B., Boyington, J. C., Moin, S. M., Gillespie, R. A., Tsybovsky, Y., Stephens, T., Vaile, J. R., Lederhofer, J., Corbett, K. S., Fisher, B. E., Yassine, H. M., Andrews, S. F., Crank, M. C., McDermott, A. B., Mascola, J. R., Graham, B. S., and Kanekiyo, M. (2020) Glycan repositioning of influenza hemagglutinin stem facilitates the elicitation of protective cross-group antibody responses. *Nat. Commun. 11* (1), 791.
(32) Mesin, L., Schiepers, A., Ersching, J., Barbulescu, A., Cavazzoni, C. B., Angelini, A., Okada, T., Kurosaki, T., and Victora, G. D. (2020) Restricted Clonality and Limited Germinal Center Reentry Characterize Memory B Cell Reactivation by Boosting. *Cell 180* (1), 92−106.
(33) Kabsch, W. (2010) XDS. *Acta Crystallogr., Sect. D: Biol. Crystallogr. 66* (Pt 2), 125−32.
(34) McCoy, A. J. (2007) Solving structures of protein complexes by molecular replacement with Phaser. *Acta Crystallogr., Sect. D: Biol. Crystallogr. 63* (Pt 1), 32−41.
(35) McCoy, A. J., Grosse-Kunstleve, R. W., Adams, P. D., Winn, M. D., Storoni, L. C., and Read, R. J. (2007) Phaser crystallographic software. *J. Appl. Crystallogr. 40* (Pt 4), 658−674.
(36) McCarthy, K. R., Watanabe, A., Kuraoka, M., Do, K. T., McGee, C. E., Sempowski, G. D., Schmidt, A. G., Kelsoe, G., and Harrison, S. C. (2017) Human memory B cells that cross-react with group 1 and group 2 influenza A viruses are abundant in adult human repertoires. *Immunity 48*, 174.
(37) Emsley, P., and Cowtan, K. (2004) Coot: model-building tools for molecular graphics. *Acta Crystallogr., Sect. D: Biol. Crystallogr. 60* (12), 2126−32.
(38) Chen, V. B., Arendall, W. B., 3rd, Headd, J. J., Keedy, D. A., Immormino, R. M., Kapral, G. J., Murray, L. W., Richardson, J. S., and Richardson, D. C. (2010) MolProbity: all-atom structure validation for macromolecular crystallography. *Acta Crystallogr., Sect. D: Biol. Crystallogr. 66* (Pt 1), 12−21.
(39) Winn, M. D., Ballard, C. C., Cowtan, K. D., Dodson, E. J., Emsley, P., Evans, P. R., Keegan, R. M., Krissinel, E. B., Leslie, A. G., McCoy, A., McNicholas, S. J., Murshudov, G. N., Pannu, N. S., Potterton, E. A., Powell, H. R., Read, R. J., Vagin, A., and Wilson, K. S. (2011) Overview of the CCP4 suite and current developments. *Acta Crystallogr., Sect. D: Biol. Crystallogr. 67* (Pt 4), 235−42.
(40) Chen, J., Lansford, R., Stewart, V., Young, F., and Alt, F. W. (1993) RAG-2-deficient blastocyst complementation: an assay of gene function in lymphocyte development. *Proc. Natl. Acad. Sci. U. S. A. 90* (10), 4528−32.
(41) Bajic, G., Maron, M. J., Adachi, Y., Onodera, T., McCarthy, K. R., McGee, C. E., Sempowski, G. D., Takahashi, Y., Kelsoe, G., Kuraoka, M., and Schmidt, A. G. (2019) Influenza Antigen Engineering Focuses Immune Responses to a Subdominant but Broadly Protective Viral Epitope. *Cell Host Microbe 25* (6), 827−835.
(42) Kuraoka, M., Schmidt, A. G., Nojima, T., Feng, F., Watanabe, A., Kitamura, D., Harrison, S. C., Kepler, T. B., and Kelsoe, G. (2016) Complex Antigens Drive Permissive Clonal Selection in Germinal Centers. *Immunity 44* (3), 542−552.

https://dx.doi.org/10.1021/acsinfecdis.0c00008
ACS Infect. Dis. XXXX, XXX, XXX−XXX